THE ASTROPHYSICAL JOURNAL, 366:474–483, 1991 January 10


# A SPECTROSCOPIC STUDY OF THE DR 21 OUTFLOW SOURCE. II. THE VIBRATIONAL $H_2$ LINE EMISSION

R. P. GARDEN
University of California, Irvine

T. R. GEBALLE
Joint Astronomy Center, Hawaii

I. GATLEY
National Optical Astronomy Observatories, Tucson

AND

D. NADEAU
University of Montreal, Canada
*Received 1990 March 6; accepted 1990 July 9*

## ABSTRACT

Large-scale mapping and high-spectral resolution profile measurements of the vibrational $H_2$ $v = 1$–$0$ $S(1)$ line are used to investigate the morphology and kinematic structure of the hot, shocked gas associated with the ultraluminous DR 21 young-stellar outflow. It is found that the $H_2$ line profiles at certain locations within the outflow possess high-velocity wings which extend to beyond 100 km s$^{-1}$ from the DR 21 rest velocity. We argue that the jets, which shock the surrounding molecular cloud medium and produce the bright $H_2$ line emission, are composed primarily of hot atomic gas which is confined by the thermal pressure of the ambient cloud medium. If this is indeed the case, it is then possible that the periodic clumping of the $H_2$ jets arise from the interaction of oblique shocks that are formed inside the jets as a result of sudden changes in the external pressure. Alternatively, if the magnetic field strength within the DR 21 cloud core is significantly greater than 30 $\mu$G, it is more likely that the jets are collimated by the magnetic pressure of the ambient cloud medium.

*Subject headings:* interstellar: molecules — nebulae: individual DR 21 — nebulae: internal motions — stars: pre–main-sequence

## I. INTRODUCTION

Molecular clouds are often seats of violent dynamical activity. This activity, as observed at infrared (Garden, Russell, and Burton 1990) and millimeter (Bally and Lada 1983) wavelengths, is believed to be fueled by high-mass star formation. In particular, the energy and momentum imparted to molecular clouds during the outflow phase of early stellar evolution (Lada 1986) can generate substantial internal motions which, in turn, alter the physical structure of the dense cloud cores in which the young stars form. One of the best probes of molecular cloud dynamics in star-forming regions is vibrationally excited molecular hydrogen ($H_2$) emission which arises predominantly from the hot shocked gas that is produced when young stellar winds collide with the surrounding ambient cloud medium.

In a previous paper (Garden *et al.* 1986; hereafter Paper I), we presented observations of the spatial distribution of $H_2$ $v = 1$–$0$ $S(1)$ line emission from the DR 21 molecular cloud. These observations showed the emission to arise from two highly collimated bipolar lobes which emanate from within the cloud core and extend in an E-W direction for over 5 pc (assuming, $D = 3$ kpc). The total luminosity in dereddened $H_2$ line emission of both lobes was determined to be $\sim 1800\ L_\odot$, thus making DR 21 one of the most luminous $H_2$ emission-line sources yet discovered in our galaxy. Line intensity ratios, measured at the peaks of line emission in both lobes, revealed that the $H_2$ is collisionally excited in a dense ($n > 10^5$ cm$^{-3}$) molecular gas at an average temperature of $T \approx 2000$ K, consistent with postshock cooling. In addition, measurements of the $S(1)$ line profiles indicated that the west lobe contains a high-velocity ($v > 60$ km s$^{-1}$), blueshifted stream of shocked gas, in contrast to the east lobe which appears to consist entirely of slower moving gas ($v < 35$ km s$^{-1}$). The momentum flux through the shocks, required to sustain the $H_2$ emission at the observed luminosity, is an order of magnitude larger than can be supplied by a stellar wind characteristic of a zero-age main sequence (ZAMS) star of luminosity comparable to that observed in the DR 21 complex ($\sim 2 \times 10^5\ L_\odot$; Harvey, Campbell, and Hoffmann 1977). Expansion of the DR 21 compact H II region is also unable to generate the required level of shock luminosity. A cloud-cloud collision, although sufficiently energetic to excite the presently observed luminosity in shocked $H_2$ line emission over an extended period of time ($> 10^5$ yr), necessitates a rather constrained geometry in order to create a flow as collimated as that observed. Therefore, we arrived at the conclusion that a powerful non–ZAMS stellar wind is the most likely driving engine. This wind presumably originates from the immediate surroundings of a luminous young-stellar object (protostar?) located deep within the DR 21 molecular cloud. It was further suggested that an inhomogeneous density distribution in the surrounding ambient molecular cloud (i.e., a dense ridge or disk) is necessary in order to collimate the wind.

In this paper (Paper II), we present more detailed observations of the shock-excited $H_2$ line emission arising from the DR 21 molecular jets; the previous observations (Paper I) being extended to higher spectral and angular resolution. In two forthcoming papers we complement the infrared data with new high-angular resolution observations of the $J = 1\text{–}0$ transitions of $^{12}CO$, $^{13}CO$, and $C^{18}O$ (Paper III), and the $J = 1\text{–}0$ and 2–1 transitions of CS (Paper IV). The results of the infrared observations are presented in § III and discussed in § IV. The main conclusions derived from these observations are summarized in § V.

## II. THE OBSERVING METHOD

The $H_2$ observations, consisting of intensity mapping and line profile measurements, were made during 1985 July 5–8 and 1986 July 10–14 at the 3.8 m United Kingdom Infrared Telescope (UKIRT) on Mauna Kea, Hawaii. The intensity of the $H_2$ $v = 1\text{–}0$ $S(1)$ line was mapped using a nominal 100 km $s^{-1}$ resolution Fabry-Perot interferometer (FP) placed in an $f/35$ beam directly in front of the facility instrument, UKT9. This instrument consists of a dewar housing a 0.8% resolution circular variable filter (CVF) and a single solid-nitrogen-cooled InSb detector. The CVF was tuned to 2.122 $\mu$m and served to block all unwanted orders of the FP. The measured resolution of the combined instrument was 130 km $s^{-1}$. At this resolution, the line was essentially unresolved at most positions observed. These measurements were obtained using a 5″ beam, with a 3″ spacing between adjacent measurements. Standard sky chopping (130″ N-S) and telescope beamswitching techniques were employed and the absolute pointing was checked after every 10 map positions. Relative positions were established by offsetting the telescope from a nearby bright star and are accurate to 2″. Wavelength calibration was determined by observing the $H_2$ $v = 1\text{–}0$ $S(1)$ line toward the bright planetary nebula NGC 7027. Line flux calibration was based on measurements of the continuum flux density of the standard G8II star, BS 8115, whose K magnitude was taken to be 1.09.

During the 1986 observing run, high-spectral resolution $v = 1\text{–}0$ $S(1)$ line profiles were measured at several positions along both outflow lobes, where the line intensity showed strong local maxima. These measurements were made using a 10″ beam and a second FP of nominal (pinhole) resolution $\sim$25 km $s^{-1}$. In this instrumental configuration, parallel light was fed through the FP, then focused through the CVF and reimaged onto the detector. The instrumental profile, measured using an argon discharge lamp, showed a reasonably symmetric Lorentzian shape of measured FWHM $\sim$35 km $s^{-1}$. Standard sky chopping (130″ N-S) and beam switching procedures were employed. Flux calibration of the profiles is not accurate due to the uncertainties introduced by the overlap of adjacent FP orders within the bandpass of the CVF. In the case of DR 21, however, the underlying continuum is negligible and no other strong emission lines lie within the CVF bandpass at 2.122 $\mu$m. We therefore contend that, although the line intensities are uncertain, the observed $S(1)$ profiles are unaffected by aliasing and give a reliable representation of the kinematics of the hot shocked gas.

Fully sampled, velocity-channel maps of the $H_2$ $v = 1\text{–}0$ $S(1)$ line emission were also obtained during the 1986 observing run. The maps were made at two fixed velocities, offset from the DR 21 rest velocity by $\Delta V = +50$ and $-50$ km $s^{-1}$, using the 35 km $s^{-1}$ resolution FP and a beam diameter of 10″.

## III. RESULTS

### a) *Morphology of the* $H_2$ *Line Emission*

A contour plot displaying the distribution of $H_2$ line flux over the entire DR 21 molecular cloud complex is shown in Figure 1. These observations reveal the same basic features as

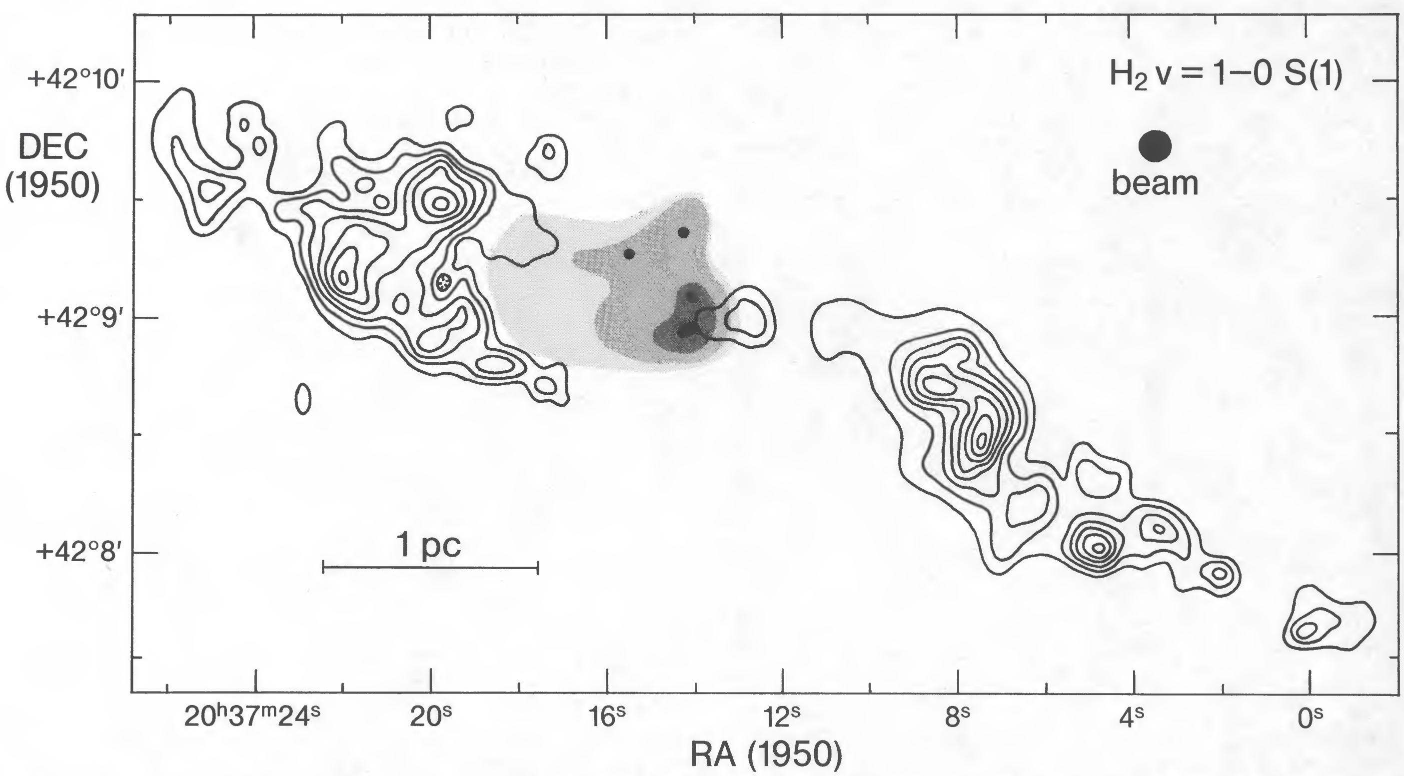


FIG. 1.—Contour map of $H_2$ $v = 1\text{–}0$ $S(1)$ line intensity in the DR 21 outflow as measured on a 3″ square grid of positions using a 100 km $s^{-1}$ resolution Fabry-Perot interferometer (FP) and a 5″ beam. The lowest intensity contour level and the contour spacing, are both $8 \times 10^{-12}$ W $cm^{-2}$ $sr^{-1}$ ($\approx 3\sigma$). The shaded area corresponds to the DR 21 compact H II region as revealed by 6 cm radio continuum emission (Roelfsema, Goss, and Geballe 1989).

already described in Paper I, namely the existence of two lobes of $H_2$ line emission oriented roughly E-W, perpendicular to the N-S major axis of the DR 21/W75S molecular cloud chain. However, the higher angular resolution afforded by the present observations reveals considerably more substructure internal to both lobes. In particular, the west lobe no longer appears as a continuous finger of emission but is now resolved into several spatially disconnected clumps which are periodically spaced along the outflow axis and tend to become both weaker and smaller with increasing outward displacement from the DR 21 cloud core. The east lobe, which is both shorter and less collimated than the west lobe, also appears to consist of several bright clumps. However, in contrast to the west lobe, the emission in the inner parts of the east lobe resembles that of a segmented shell which is oriented roughly orthogonal to the E-W axis of the main outflow.

Garden, Russell, and Burton (1990) have extended the investigation of the morphological structure of the DR 21 outflow lobes to a higher angular resolution than is presented here. These authors have obtained an image of the DR 21 outflow source in the $H_2$ $v = 1$–$0$ $S(1)$ line at 2″ resolution, more than twice the angular resolution of the map presented in Figure 1. This image shows that the main intensity peaks discussed above break up into even smaller subclumps. However, these subclumps appear to be tightly grouped with each grouping having the same interclump spacing as displayed in Figure 1. We therefore contend that the distribution of clumps in Figure 1 is an intrinsic property of the DR 21 outflow rather than a reflection of the spatial resolution used to make the observations. This is an important conclusion since the clump spacing is used in § IV*c* to calculate specific properties of the DR 21 outflow. The main reason for including the lower angular resolution map in this paper is that it is better matched to the angular resolution of the beam used to measure the $H_2$ line profiles.

### *b*) *The Importance of Extinction*

As discussed in Paper I and confirmed by our $C^{18}O$ observations (to be discussed in Paper III), the foreground visual extinction decreases rapidly from more than 100 mag at the DR 21 cloud core to less than 30 mag at the innermost peaks of the $H_2$ lobes. Although the near infrared extinction associated with the extended $H_2$ outflow lobes is significant ($1 < A_{2.12\,\mu m}(\mathrm{mag}) < 3$) and undoubtedly blocks much of the diffuse $H_2$ emission, it is not of sufficient magnitude to seriously affect the intrinsic morphology of the brightest emission-line peaks. We therefore argue that Figure 1 gives a true representation of the intrinsic distribution of shock-excited $H_2$ line emission. A similar conclusion has been reached by Nadeau and Geballe (1990, in preparation) from detailed measurements of the $H_2$ $S(1)$ to $Q$-branch intensity ratio at several positions, both along the inner edges of, and at several peak and off-peak positions along, the $H_2$ outflow lobes. Additional evidence in support of this claim derives from the morphological similarity exhibited between the near-infrared $H_2$ and the high-velocity CO (Paper III) and $HCO^+$ (Garden and Carlstrom 1991, in preparation) emission which would not result if the near-infrared emission were seriously affected by heavy foreground extinction.

### *c*) *The* $H_2$ *Line Profiles*

Profiles of the $H_2$ $v = 1$–$0$ $S(1)$ line, measured at 12 different locations across the $H_2$ lobes, are presented in Figure 3. The positions at which these profiles were measured are indicated in Figure 2 and a comparison of the main profile parameters is given in Table 1. As can be seen from these figures, the $S(1)$ profiles at different locations in the source show distinct differences in the velocity of peak line emission and width at half-maximum intensity. On average, the velocities of peak line emission in the west lobe are blueshifted by $\sim 10$ km s$^{-1}$ relative to those of the east lobe which, in turn, are blueshifted by 3–5 km s$^{-1}$ relative to the DR 21 rest velocity ($\sim -2.5$ km s$^{-1}$). Thus, the outflow in DR 21 is not strongly bipolar in velocity. It should be remembered, however, that the outflow axis is oriented almost perpendicular to the line of sight thus making it difficult to detect a bipolar velocity field.

An attempt has been made to deconvolve the observed $S(1)$ velocity profiles using the instrumental profile derived from measurements of an argon arc-lamp line. A one-dimensional maximum-entropy (MEM) deconvolution algorithm was employed (Willingale 1981; Skilling and Bryan 1984), the results of which are shown along with the observed profiles in

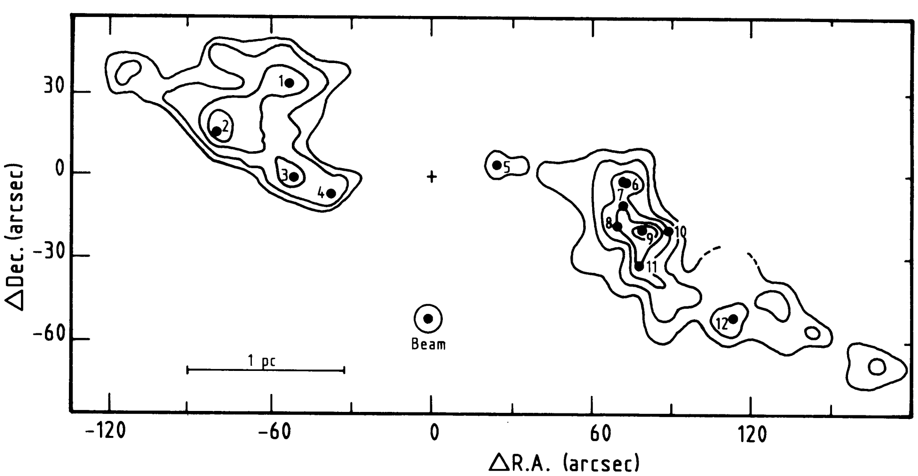


FIG. 2.—Contour map of the $H_2$ $v = 1$–$0$ $S(1)$ line in the DR 21 outflow as measured on a 5″ square grid of positions using a 100 km s$^{-1}$ resolution FP and a 10″ beam. Indicated on this map are the positions at which the FP profiles shown in Figure 3 were measured. The map center (0,0) is at R.A. = $24^h37^m14^s.8$, Decl. = 42°08′56″ (1950) and lies close to the centroid of the DR 21 high-velocity CO outflow (Paper III). The offset of each position from the map center is given in Table 1.

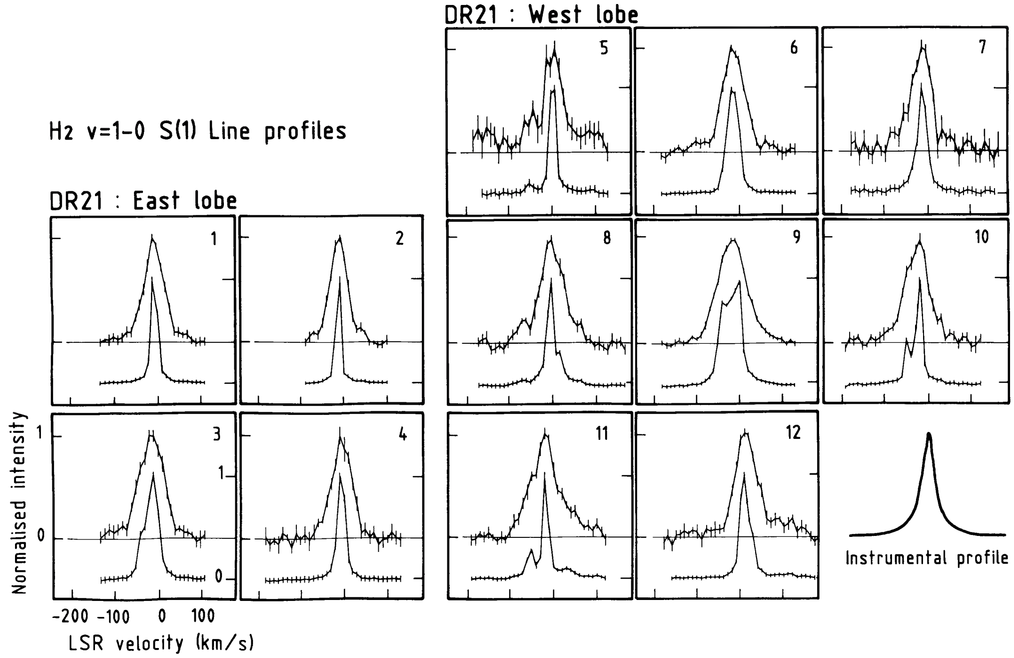


FIG. 3.—Observed (*upper*) and deconvolved (*lower*) $H_2$ $v$ = 1–0 $S$(1) profiles for the DR 21 outflow source as measured using a FP with a 10″ beam and 35 km $s^{-1}$ resolution at the positions indicated in Fig. 2. The profile parameters are summarized in Table 1.

Figure 3. From the deconvolved profiles it is clear that, toward several positions in the west lobe, the $S$(1) line emission extends to velocities of order 100 km $s^{-1}$ on either side of the line core, while toward the east lobe, the profile is quite narrow and exhibits no apparent emission beyond 20 km $s^{-1}$ from the line core. Furthermore, several of the deconvolved profiles in the west lobe appear to be multicomponent with emission features separated by velocity displacements in the range 20–30 km $s^{-1}$. In conjunction with the $H_2$ intensity map (Fig. 1), these results present convincing evidence for significant differences of both the geometry and internal kinematics between the east and west lobes of the DR 21 outflow source.

Not only does the line width and shape of the $S$(1) profile vary from position to position across the $H_2$ lobes, but the velocity of peak line emission also varies. As shown in Figure 3 and indicated in Table 1, the velocity of peak line emission in the west lobe is initially redshifted close to the cloud core, then becomes blueshifted midway along the lobe, and finally turns redward again at the outer extremity of the lobe. The maximum velocity shift between adjacent clumps is of order 30 km $s^{-1}$. The existence of an oscillating radial velocity field along the western lobe of $H_2$ line emission is further supported by the appearance of Figure 4 which displays an overlay of the red ($v_r$ = +47 km $s^{-1}$) and blue ($v_b$ = −53 km $s^{-1}$) $H_2$ $v$ = 1–0 $S$(1) emission at velocity displacements ±50 km $s^{-1}$ from the DR 21 rest velocity (∼ −2.5 km $s^{-1}$). This figure clearly shows that the emission associated with the west $H_2$ lobe oscillates in radial velocity with outward displacement along the lobe, in agreement with the individual line profile measurements. In contrast to the west lobe, the velocity of

TABLE 1

$H_2$ $\sigma$ = 1–0 $S$(1) PROFILE PARAMETERS

| | | | | OBSERVED | | | DECONVOLVED | |
|---|---|---|---|---|---|---|---|---|
| POSITION | OFFSET[a] (arcsec) | | FLUX[b] (W $cm^{-2}$) | $V_{lsr}$(Pk)[c] (km $s^{-1}$) | FWHM (km $s^{-1}$) | $B/R$[d] | FWHM (km $s^{-1}$) | FWZI[e] (km $s^{-1}$) |
| 1 .................... | 54 | 34 | $2.9 \times 10^{-20}$ | −8 | 52 | 1.35 | 20 | 95 |
| 2 .................... | 80 | 15 | 4.0 | −10 | 48 | 1.05 | 15 | 60 |
| 3 .................... | 52 | −1 | 2.1 | −17 | 65 | 1.00 | 35 | 110 |
| 4 .................... | 38 | −7 | 2.0 | −5 | 53 | 1.07 | 23 | 105 |
| 5 .................... | −23 | 4 | 0.9 | +4 | 45 | ? | 23 | >140* |
| 6 .................... | −72 | −4 | 3.6 | −17 | 63 | 0.81 | 35 | 115 |
| 7 .................... | −70 | −11 | 2.2 | −14 | 57 | 0.94 | 26 | 140 |
| 8 .................... | −68 | −22 | 2.7 | −8 | 63 | 1.07 | 25 | 175* |
| 9 .................... | −78 | −24 | 5.3 | −21 | 80 | 1.02 | 58 | 230* |
| 10 .................... | −85 | −24 | 2.7 | −22 | 60 | 1.32 | 23 | 140* |
| 11 .................... | −76 | −34 | 2.9 | −19 | 65 | 0.71 | 27 | 160* |
| 12 .................... | −112 | −52 | 3.0 | +16 | 61 | 0.74 | 25 | 105 |

[a] From R.A. = $20^h37^m14^s.8$, Decl. = 42°08′56″ (1950).
[b] In 10″ aperture, integrated over profile, uncertainty typically ±15%.
[c] Uncertainty typically ±5 km $s^{-1}$.
[d] Ratio of integrated line flux to blue and red of $V_{lsr}$(Pk).
[e] Asterisk denotes multiple components in deconvolved profile.

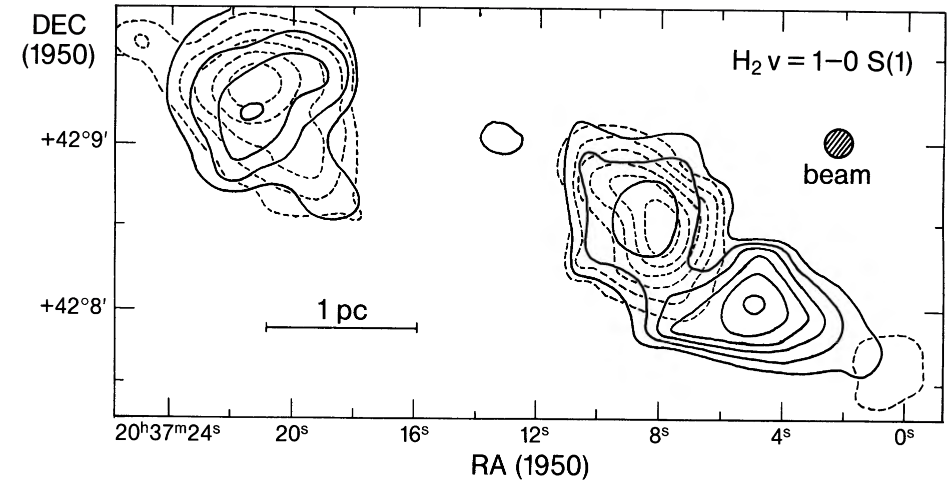


FIG. 4.—Blue ($\Delta v = -50$ km s$^{-1}$, *solid line*) and red ($\Delta v = +50$ km s$^{-1}$, *broken line*) velocity-channel maps of $H_2$ $v = 1$–0 $S(1)$ line emission as measured using a 35 km s$^{-1}$ resolution FP and a beam size of 10″.

peak line emission in the east lobe appears to be less organized with various velocity components intermixed in a rather complex fashion.

It is interesting to compare the width of the broad $S(1)$ profile observed toward the west lobe of the DR 21 $H_2$ source with that of the $S(1)$ profile observed toward the well-studied, high-velocity outflow in Orion (Nadeau, Geballe, and Neugebauer 1982; Scoville *et al.* 1982). In order to facilitate such a comparison, a velocity-resolved profile of the $S(1)$ emission toward Orion Peak 1 was obtained on 1986 January 1–2, using an instrumental set-up identical to that employed for the DR 21 measurements. A comparison of the DR 21 and Orion $S(1)$ profiles shows that both possess similar widths at half-maximum intensity ($\sim 30$ km s$^{-1}$) and are of comparable velocity extent (FWZI > 150 km s$^{-1}$). These observations therefore suggest that the high-velocity $H_2$ $v = 1$–0 $S(1)$ emission associated with the DR 21 molecular outflow is similar in nature to that previously identified with the Orion outflow. More importantly, these observations indicate that the Orion outflow source is not unique with regard to its ultrahigh velocities.

### *d) Physical Properties Derived from the* $H_2$ *Line Emission*

The mass of hot $H_2$ can be calculated knowing the total line flux at Earth, $F$, for a source at distance, $D$, as follows

$$M(H_2, T_x) = \frac{Z(T_x)\exp[T_u/T_x]m(H_2)}{G(J)h\nu A} F[4\pi D^2] , \quad (1)$$

where $m(H_2)$ is the mass of $H_2$ molecule, $T_u$ is the temperature of the upper level, $T_x$ is the excitation temperature, $G(J) = (2J+1)g_{\rm spin}$ is the statistical weight of the level ($g_{\rm spin} = 3$ for orthohydrogen and 1 for parahydrogen), $Z(T_x)$ is the partition function (taken to be 50 at $T_x = 2000$ K), $F$ is the line flux, and $D$ is the distance to the source. For the $v = 1$–0 $S(1)$ line, this gives

$$M(H_2)_{\rm hot} = 1.5 \times 10^{-3}[L_{v=1-0\,S(1)}/L_\odot]\ M_\odot . \quad (2)$$

As discussed in Paper I, the reddening to the $H_2$ emission-line region was calculated by comparing the observed ratio of the $S(1)$ to $v = 1$–0 $Q$-branch lines at the positions of peak emission in the east and west lobes with that predicted from theory. The total dereddened line luminosity was then calculated assuming that the same reddening applies over the remainder of the emission-line lobes. Since at least 75% of the total $S(1)$ line flux arises from the brightest east and west peaks, this last assumption is not too important. Thus, from Paper I we have, $L_{v=1-0\,S(1)} = 180(D/3\ {\rm kpc})^2\ L_\odot$. Using equation (2), this gives $M(H_2)_{\rm hot} = 0.27(D/3\ {\rm kpc})^2\ M_\odot$ for the mass of hot $H_2$. Overall, we believe that our estimate for $L_{v=1-0\,S(1)}$, and hence $M(H_2)_{\rm hot}$, is probably good to within a factor of 3.

The mass transfer rate through the shocks that give rise to the luminous $H_2$ line emission can now be estimated simply by dividing the total mass of hot $H_2$ by the average lifetime of a $H_2$ molecule in the vibrational state. The time spent by a $H_2$ molecule in the hot ($T > 1500$ K) post-shock zone can be calculated as follows

$$t_{\rm hot} = [N(H_2)_{\rm hot}/n(H_2)_{\rm ps}]/v_{\rm shock} . \quad (3)$$

Inserting the average values $N(H_2)_{\rm hot} = 10^{19}$ cm$^{-2}$ (Paper I), $n(H_2)_{\rm ps} = 10^5$ cm$^{-3}$ and $v_{\rm shock} = 30$ km s$^{-1}$, results in a shocked layer of thickness $\approx 10^{14}$ cm and a lifetime for vibrationally excited $H_2$ of $t_{\rm hot} \approx 1$ yr. The mass transfer rate through the shocks is then $\dot{M}_{\rm shock} = M(H_2)_{\rm hot}/t_{\rm hot} \approx 0.3(D/3\ {\rm kpc})^2\ M_\odot\ {\rm yr}^{-1}$. Due to the simplicity of this argument, in conjunction with the other uncertainties discussed above, this result is probably only good to within an order of magnitude. For comparison, we shall show in Paper (III) that the mass-loss rate in swept-up ambient gas, calculated from observations of high-velocity CO line emission, is of order $\dot{M}_{\rm su} \approx 10^{-2}\ M_\odot\ {\rm yr}^{-1}$. Even if $\dot{M}_{\rm shock}$ were to be reduced by an order of magnitude, it would still represent an enormous mass transfer rate, several orders of magnitude larger than has been calculated for other known molecular outflow sources (Lada 1986). Providing that the outflow has retained its present vigor for most of its lifetime ($\sim 5 \times 10^4$ yr; see Paper III), the above mass transfer rate suggests that a large part ($\sim 10\%$) of the DR 21 molecular cloud has been processed through shocks. As will be discussed in Paper IV, these shocks may significantly alter the chemical composition of the ambient cloud medium.

## IV. DISCUSSION

### *a) Comparison with Other Observations*

Thermal continuum observations (Harvey *et al.* 1986) from 2.2 to 300 $\mu$m show that the DR 21 core is the brightest far-infrared source in the DR 21/W75S complex. One of the most striking results derived from these observations is the much greater E-W than N-S extent of the DR 21 source, as well as the elevated temperature to the east and possibly to the west of the main luminosity peak. Conversely, the optical depth maps shows a higher dust column density along the N-S direction. Harvey *et al.* suggest that these asymmetries may be related to the DR 21 outflow phenomenon, in which case the higher dust temperatures to the east and west may represent regions of enhanced deposition of mechanical energy due to dissipation at shock fronts. The spatial correlation of warm dust and strong vibrationally excited $H_2$ line emission certainly favors such a scenario. Moreover, the N-S elongation of enhanced dust column density exhibits the correct orientation if it were to arise from a ridge of dense material which acts to collimate the predominantly E-W oriented molecular flows. As will be discussed in Paper IV, our observations of CS $J = 1$–0 and $J = 2$–1 line emission confirm the existence of the ridge and its N-S orientation.

The 20 $\mu$m continuum emission shows a broad resemblance to the 5 Ghz radio continuum observations of Harris (1973) and Roelfsema, Goss, and Geballe (1989). Such a resemblance is commonly found in regions where the mid-infrared continuum arises primarily from warm dust on the edge of a luminous H II region. The radio emission, which shows a sudden cutoff at the western boundary and a much more gradual decrease to the east, is a prime example of a blister-type H II region (Tenorio-Tagle 1979) in which the ionized gas is confined on one side by the molecular cloud and expands freely outward on the other side. Embedded within the DR 21 compact H II region are five or more bright peaks of radio continuum emission, reminiscent of a compact cluster of O stars. A superposition of the radio continuum emission (Roelfsema *et al.* 1989) on our map of integrated $H_2$ line emission is shown in Figure 1. It is interesting to note how well the radio emission fills the central hole in the $H_2$ line emission. As discussed by Garden, Russell, and Burton (1990), it is possible that some ($\sim 10\%$) of the $H_2$ line emission on the eastern side of the DR 21 H II region is excited in a photodissociation region at the boundary of the H II region. Although lacking evidence, we find it hard to accept that the location of the O star cluster at the center of the DR 21 high-velocity outflow is pure coincidence. Instead, we speculate that the young O star cluster must somehow play a role in generating the complex outflow phenomena seen in this region.

### b) *The Outflow Energetics*

It is interesting to compare the total luminosity radiated in shock-excited $H_2$ line emission with the bolometric luminosity of the DR 21 star-forming region, as the ratio of these two quantities can be used to parameterize the relative importance of shock heating/cooling to the overall energy budget. For the DR 21 outflow source, $L_{\rm bol} \approx 2 \times 10^5\ L_\odot$ (Harvey, Campbell, and Hoffmann 1977) and $L(H_2) \approx 1800\ L_\odot$ (Paper I) giving $L(H_2)/L_{\rm bol} \approx 0.01$. This value of $L(H_2)/L_{\rm bol}$ is comparable to those derived for the analogous outflow sources associated with the NGC 2071 (Lane and Bally 1986) and Orion (Beckwith 1983) star-forming regions. Thus, although the efficiency of generating strong $H_2$ line emission probably depends on both the stage of evolution of the outflow and the density distribution of the surrounding cloud, it appears that for a massive outflow in its most active phase, a reasonable estimate for the luminosity in shocked $H_2$ line emission is $\sim 1\%$ of the bolometric luminosity of the central source. The luminosity ratio for all shock coolants (including far-infrared CO and O I emission) is probably 2 to 3 times higher (Geballe and Garden 1987).

### c) *The* $H_2$ *Jets and Their Collimation*

The evolution of stellar winds in a dense, inhomogeneous molecular cloud medium has been studied theoretically by Canto and Rodriguez (1980), Konigl (1982), and Canto *et al.* (1988). These authors show that originally spherical wind bubbles can evolve into ovoids if the cooling time of the shocked wind is sufficiently short, or into De Laval nozzles if radiative cooling is inhibited and adiabatic conditions prevail.

As shown by Norman and Silk (1980) and further discussed by Dyson (1984), the condition for the formation of an adiabatic stellar wind within a dense molecular cloud is that the stellar wind velocity $v_w$ must be greater than a critical velocity $v_c$, where

$$v_c \approx 85 R^{-2/157} \dot{M}_6^{16/157} n_0^{14/157}\ \mathrm{km\ s^{-1}}\ , \tag{4}$$

where $R$ is the wind radius in pc, $\dot{M}_6$ the stellar mass-loss rate (in units $10^{-6}\ M_\odot\ \mathrm{yr}^{-1}$), and $n_0$ the ambient number density (assumed uniform). Although the above equation is specifically for a spherical wind the result is not significantly changed for the case of a bipolar outflow, providing all of the wind is diverted into the bipolar lobes.

For the DR 21 outflow we take $R \approx 3$ and $n_0 \approx 10^4$. According to the analysis of Norman and Silk (1980), this gives $200 < v_c < 400$ km s$^{-1}$ for $10^{-6} < \dot{M}_w < 10^{-3}$. It is impossible to give an exact value for the stellar mass-loss rate since the stellar wind has not yet been identified. However, we can obtain an upper limit for $\dot{M}_w$ from a comparison of the momentum flux in the stellar wind and swept-up ambient gas. As shown by Kwok and Volk (1985), if the wind interaction is adiabatic, the momentum in the swept-up ambient gas can be significantly larger (up to several orders of magnitude) than the momentum in the stellar wind. Thus, for an energy-driven wind

$$\dot{M}_w = \frac{\dot{M}_{\rm su}}{\epsilon}\left(\frac{v_{\rm su}}{v_w}\right) \tag{5}$$

where $\epsilon > 1$. From the results of this paper and Paper (III), we take $\dot{M}_{\rm su} \approx 10^{-2}\ M_\odot\ \mathrm{yr}^{-1}$ and $v_{\rm su} \approx 30$ km s$^{-1}$. Since $v_w \geq v_c$ for an energy-driven wind, this implies that $v_{\rm su}/v_w \approx 0.1$ and $\dot{M}_w \approx 10^{-3}/\epsilon$. For typical values of $\epsilon$ (i.e., $1 < \epsilon < 10$), equation (4) then gives $300 < v_c < 400$ km s$^{-1}$. Thus, the condition for the formation of an adiabatic wind within the DR 21 outflow system is that the stellar wind velocity must be greater than $\sim 300$ km s$^{-1}$, else the wind will rapidly cool and the outflow will be momentum driven.

#### i) *Energy-Driven Jets*

In the following analysis we assume that $v_w > 300$ km s$^{-1}$. Although this is a factor of 3 larger than the highest velocity shifts seen in our $H_2$ line profiles, we do not consider this to be a serious problem since the $H_2$ emission originates primarily from swept-up gas along the walls of the outflow and not from the stellar wind itself. Furthermore, the extremely collimated appearance of the $H_2$ emission suggests that the outflow axis is oriented at a large angle to the line of sight. This then implies that the observed $H_2$ profiles are modified by projection effects which, when accounted for, could easily result in intrinsic shock speeds 2 to 3 times higher than measured. As a final argument for an energy-driven wind, we return to the O star cluster located at the center of the DR 21 outflow system. If, as suggested by the radio observations, these O stars have already approached the main sequence, they should possess surface winds with velocities exceeding 1000 km $s^{-1}$. It is therefore possible that the high-velocity stellar wind required to drive the extended outflows may originate from these young O stars. Since the stellar wind is expected to be either ionic or atomic in form, it is not directly revealed by the $H_2$ observations but may be visible using high-sensitivity measurements of infrared hydrogen recombination lines or the 21 cm line of atomic hydrogen.

If the DR 21 outflows are indeed energy driven, and hence adiabatic, the possibility arises that the physical conditions in these flows may bear some resemblance to the physical conditions thought to be characteristic of extragalactic radio jets. The evolution of an adiabatic wind bubble in an anisotropic density distribution has been studied analytically by Blandford and Rees (1974), Konigl (1982), and Sanders (1983), and numerically by Norman *et al.* (1981, 1986), Hardee (1982), and Wilson and Falle (1985), to name but a few. It is important to note, however, that these studies strictly apply to extragalactic plasma jets and must be scaled down by tens of orders of magnitude in both power and linear extent in order to facilitate direct comparison with molecular flows..

An interesting case at hand is that of a jet confined by a power-law density profile in the ambient medium of a flattened cloud. Such a case was first discussed by Blandford and Rees (1974), who developed the twin-exhaust model to explain the collimation of bipolar jets in radio galaxies and quasars. Norman *et al.* (1986) note that because the basic physics underlying the twin-exhaust model are effectively scale invariant, this simple model may be used to explain the formation of bipolar jets for a broad range of astrophysical environments. Making use of this fact, Konigl (1982) has applied the twin-exhaust model to bipolar molecular outflows, where the energy source is a young star with a strong stellar wind, and the confining agent is a dense molecular cloud. This model has also been used to explain the highly collimated and clumpy structure of optical/radio jets associated with young T Tauri stars (Mundt, Brugel, and Burke 1987).

The twin-exhaust model works as follows. As the hot adiabatic bubble of stellar wind gas is accelerated along the direction of least resistance (i.e., parallel to the minor axis of the flattened cloud), the interaction layer becomes subject to the Rayleigh-Taylor instability which leads to the formation of a De Laval nozzle. If the external pressure obeys a power-law of form $P_{\rm ext} \propto z^{\alpha}$, where $z$ is the radial displacement along the jet axis, pressure confinement is impossible if $\alpha < -2$ since the jet pressure cannot fall as fast as the pressure in the surrounding ambient cloud medium (Konigl 1982; Sanders 1983). However, if $\alpha > -2$, a jet with initially greater internal than external pressure (i.e., an under-expanded jet) could effectively "break-free" and expand, with the internal pressure dropping faster than the pressure in the ambient cloud medium, until the latter pressure catches up and the jet is once again reconfined. As the jet is compressed, its internal pressure overshoots the ambient cloud pressure and the cycle of events is repeated. Thus, the sudden expansion of an under-expanded jet on ejection from the De Laval nozzle can set up a train of compression and rarefaction waves that propagate along the length of the jet. This simple analytical result is supported by detailed numerical simulations of the propagation characteristics of supersonic, pressure-confined jets (see Norman *et al.* 1986, and references therein). These simulations indicate that perturbations at the jet boundary, induced either by sudden changes in the external cloud pressure or the growth of long-wavelength Kelvin-Helmholtz instabilities, can generate a succession of oblique shocks internal to the jet. Furthermore, Rayleigh-Taylor instability of the central wind cavity can temporarily close off the De Laval nozzle which results in an intermittent flow (Blandford and Konigl 1979) and can introduce large chunks of dense cloud gas into the wind, which may then be shocked. We therefore deduce from the above that a pressure-confined jet should exhibit a rich morphological and kinematic structure along its entire length.

For low external pressures, and hence low Mach numbers, laboratory experiments indicate that these quasi-periodic internal shocks, or "Mach disks," show a tendency to be regularly spaced along the jet with a separation given by (Prandtl 1904)

$$L_j = r_j M_j , \tag{6}$$

where $M_j$ is the Mach number and $r_j$ the jet radius. Moreover, as the periodic shocks originate from an inward compression, they tend to sustain the collimation of the jet out to considerable distances from the driving source. For higher external pressures and Mach numbers, Prandtl's empirical relationship breaks down and a saturation wavelength, $L_j \sim 2r_j$, is obtained due to the formation of strong oblique shocks internal to the jets (e.g., Hartmann and Lazarus 1941).

The resemblance of the experimental/theoretical predictions with the $H_2$ observations of the DR 21 outflows, namely the presence of regularly spaced emission-line knots within the western jet, suggest that this jet may indeed be collimated by some form of pressure confinement. If so, it should be possible, using the above empirical relationships, to estimate the intrinsic jet width. However, this requires that we know both the oscillation wavelength (i.e., the knot spacing) and the jet Mach number. To calculate the latter, we assume that the jet is composed mainly of atomic hydrogen (Russell 1990), most of which derives from the dissociation of molecular hydrogen in fast shocks. If this is indeed the case, then the gas within the jet must also be heated by these same shocks. Since some cooling may have occurred between the hot shocks, as seen in the vibrational $H_2$ lines, and the postshock gas, we expect the temperature of the warm atomic gas to lie somewhere between a few thousand and a few hundred K. For the purpose of the following discussion, we assume $T_j \approx 500$ K, but note that this estimate is highly uncertain. If the jet is composed mainly of shocked atomic gas at this temperature, then the sound speed of the jet material is $C_j = (\gamma kT/\mu m_{\rm H})^{1/2} \approx 2$ km $s^{-1}$, and the Mach number is $M_j \approx 50(v_j/100$ km $s^{-1})$. Now, referring back to the laboratory results cited in the previous paragraph, the following limits are obtained for the jet radius: $0.02(v_j/100$ km $s^{-1})^{-1}(L_j/1.0$ pc$) < r_j < 0.5(L_j/1.0$ pc$)$, where $L_j$ is the oscillation wavelength or knot spacing. Thus, if the DR 21 jets are indeed pressure confined, the intrinsic radius of the jet may be quite small (0.02–0.5 pc) compared to the jet length ($\sim$3 pc for the western $H_2$ jet). This prediction agrees with the $H_2$ emission-line image displayed in Plate 2 of Garden, Russell, and Burton (1990), in which the width of the western jet is seen to be less than 10" (i.e., $r_j < 0.1$ pc). In this picture, one may well expect the De Laval nozzles to form at the outer boundary of the dense cloud core, where the radial pressure gradient is steepest. Furthermore, as a result of the sudden acceleration on emergence from the De Laval nozzle, the shocks are expected to be strongest in the inner regions of the flow, becoming weaker with increasing distance along the jet as a result of damping by viscous forces. These general features, (i.e., the narrow, clumpy jet) fit the observations rather well and thus give considerable support to the adiabatic jet model. Of course, if the jet were entirely adiabatic it would be invisible in $H_2$ line emission since, by definition, there would be no radiative shocks. Since there are strong radiative shocks associated with the DR 21 outflow, this implies that in order for the jets to remain adiabatic, the energy radiated by the shocks at any position along the jet must be significantly less than the internal energy of the jet at that position. Obviously, this assumption breaks down at the jet terminus where the jet directly impacts the ambient cloud medium thus converting most of its kinetic and thermal energy into line radiation.

So far, the argument in favor of the adiabatic jet model hinges on morphological evidence. It is now necessary to consider whether such a model can also account for the observed physical properties of the DR 21 molecular jets before invoking its validity. In order to do this, we construct a simple dynamical model for the DR 21 jets in a manner analogous to that discussed by Lane and Bally (1986) for the NGC 2071 outflow. The adiabatic jet is modeled as a collimated, pressure-confined flow of shocked atomic gas with a particle density $n_j$ and a velocity $v_j$ in an axially symmetric, linear channel of radius $r_j$. The jet material is assumed to derive from a stellar (or circumstellar) wind characterized by a spherical mass-loss rate $\dot{M}_w$, of which a fraction $\eta$ ($\sim$0.5 for a bipolar geometry) is diverted into the jets. The mechanical luminosity of the jets can then be expressed as follows.

$$L_m = \tfrac{1}{2}\eta \dot{M}_w v_j^2 \; . \tag{7}$$

For a pressure confined jet, the condition for pressure confinement can be written as

$$n_c T_c = n_j T_j \, , \tag{8}$$

where, $n_c$, $n_j$ and $T_c$, $T_j$ are the ambient cloud/jet densities and temperatures, respectively. In addition, for linear flow through a cylinder, the following relationship results.

$$n_j = \frac{\eta \dot{M}_w}{\pi \mu m_{\rm H} r_j^2 v_j} \; . \tag{9}$$

Combining equations (5), (6), and (7) then gives (see Lane and Bally 1986)

$$\dot{M}_w = \frac{1}{\eta}(2^{1/2}\pi\mu m_{\rm H})^{2/3}\left[\frac{(n_c T_c)}{T_j}\right]^{2/3} r_j^{4/3} L_m^{1/3} \, , \tag{10}$$

and

$$v_j = \left[\frac{2}{\pi \mu m_{\rm H}}\right]^{1/3}\left[\frac{L_m T_j}{n_c T_c}\right]^{1/3} r_j^{-2/3} \; . \tag{11}$$

At the "head" of the jet, where the supersonic flow collides with the ambient cloud medium, the cloud shock velocity $v_c$ is related to the jet velocity $v_j$ as follows

$$v_c = [n_j/n_c]^{1/2} v_j = [T_c/T_j]^{1/2} v_j \tag{12}$$

Finally, in order to link the model predictions with the observations, it is assumed that when the jet collides with the surrounding ambient cloud a significant portion ($\kappa$) of the wind mechanical luminosity is converted into shock-excited $H_2$ line emission, thus

$$L_m = \kappa L({\rm H_2}) \; . \tag{13}$$

Substituting the above relation into equations (8) and (9) and expressing the result in astrophysical units gives

$$\dot{M}_w = 1.8 \times 10^{-5}[(n_c T_c)/T_j]^{2/3}[\kappa L({\rm H_2})]^{1/3} r_j^{4/3} \, M_\odot \ {\rm yr}^{-1} \, , \tag{14}$$

and

$$v_j = 51\left[\frac{\kappa L({\rm H_2}) T_j}{n_c T_c}\right]^{1/3} r_j^{-2/3} \ {\rm km\ s^{-1}} \; . \tag{15}$$

For the DR 21 jets, the following values are chosen: $5 \times 10^3 < n_c < 5 \times 10^4$ cm$^{-3}$, $100 < T_j < 1000$ K, $T_c = 30$ K, $r_j = 0.1$ pc, $\kappa = 1$ and $L(H_2) = 1800 \ L_\odot$. The value of $n_c$ is obtained with reference to the CS observations discussed in Paper IV; $T_c$ is derived from the peak CO antenna temperature on the assumption that the $J = 1$–0 line is thermalized as discussed in Paper III; $r_j$ is taken from Plate 2 of Garden, Russell, and Burton (1990); $L(H_2)$ is obtained from the $v = 1$–0 $S(1)$ $H_2$ observations presented in Paper I; and $T_j$ is derived assuming the atomic gas internal to the jet is significantly heated by the wind/cloud shocks. The uncertainty in both the cloud density and jet temperature is approximately a factor of 10. Using the above values we thus obtain $10^{-4} < \dot{M}_w < 10^{-2} \ M_\odot$ yr$^{-1}$ and $100 < v_j < 500$ km s$^{-1}$ for the wind mass-loss rate and jet velocity, respectively. Consequently, from equation (10) our best estimate for the cloud shock velocity is $50 < v_c < 90$ km s$^{-1}$. The predicted range in mass-loss rate compares favorably with the mass-loss calculations presented in § III*d*. In addition, the predicted range of cloud shock velocity matches the widths of the high-velocity CO profiles (Paper III). The shock-excited $H_2$ line profiles, which are generally broader than the CO profiles, probably arise closer to the jet/cloud boundary where the velocities are higher. As a final test of the adiabatic jet model, we note that the model predicts extremely high velocities within the jet flow ($100 < v_j < 500$ km s$^{-1}$). However, it is important to note that when comparing $v_j$ with the observed line widths, the above model predictions should be reduced by a factor of 2 to 3 in order to account for projection effects. With this in mind, we find good agreement between the model predictions and the $H_2$ profiles which in some places extend to beyond 100 km s$^{-1}$ from the line core. Recent 21 cm observations of atomic hydrogen (Russell 1990) also show evidence for high-velocity gas shifted by >90 km s$^{-1}$ from the cloud rest velocity. It therefore appears that most of the observations available to date on the DR 21 outflow lend strong support, in terms of both morphology and kinematics, for the adiabatic jet model.

#### ii) *Momentum-Driven Jets*

Although the above analysis suggests that the DR 21 jets are probably energy-driven, it is important to note that the assumption of adiabaticity may not strictly apply to the physical conditions characteristic of dense molecular clouds where rapid deceleration and efficient cooling take place. Indeed, velocity profile measurements of the infrared Brackett H I recombination lines, which are believed to arise from the ionized circumstellar winds of young or currently forming stars (Alonso-Costa and Kwan 1989, and references therein), indicate that the terminal velocities of most young stellar winds are less than 300 km s$^{-1}$. If the same were true of the DR 21 stellar wind then, according to the above analysis, the outflow would be momentum driven. In the case of a momentum-driven outflow the shocked wind region degenerates into a thin, cool, dense shell and the focusing mechanism of the adiabatic model (i.e., the formation of a De Laval nozzle) ceases to work (Tenorio-Tagle and Rozyczka 1986). Canto (1980) has proposed a model for the collimation of a stellar wind in which efficient cooling takes place. Again, a flattened cloud density distribution is introduced in order to perform the initial collimation of an originally spherical stellar wind bubble. The important difference between Canto's model and the adiabatic model is that the wind strikes the outer wind-swept shell at large angles thus inducing material flow along the walls of the stellar wind bubble which in turn helps to collimate the wind via momentum conservation. Rozyczka and Tenorio-Tagle (1985) have used two-dimensional hydrodynamic simulations, based on the Canto collimation concept, to follow the non-steady state evolution of a stellar wind within a dense anisotropic molecular cloud. Their numerical results agree with those of the much simpler Canto model. However, by incorporating evolution of the system they find that extremely collimated jets can form and propagate large distances from the power source. Furthermore, at the sides of the elongated shell, strong shear motions develop on the border between the shell and the shocked wind region which result in turbulent motions and possibly the entrainment of clumps into the flow. Long-wavelength Kelvin-Helmholtz instabilities are also prone to develop under a wide range of physical conditions and can lead to periodic oscillation of the jet boundaries in a manner similar to the adiabatic jet model. It is therefore difficult to differentiate between the adiabatic and cooling models without a direct measurement of the stellar wind velocity.

#### iii) *Magnetic Confinement*

In the above discussion we have assumed that the jets are confined by the thermal pressure of the surrounding molecular cloud medium. An alternative scenario that should also be investigated is the confinement of the jets by the magnetic pressure associated with the magnetic fields that presumably thread the DR 21 molecular cloud. If magnetic pressure is to play an important role in the confinement of the jets, the direction of the magnetic field should be parallel to the jet axis (i.e., E-W). A test of this prediction requires a direct measurement of the polarization vectors of the $H_2$ line itself or of the continuum from background stars (Hough *et al.* 1987). Since no such measurements have yet been made toward this region, we can at this stage, only make a crude guess as to the feasibility of this scenario.

An order of magnitude estimate of the importance of magnetic fields for confining the jets can be obtained by simply equating the thermal pressure within the jets to the magnetic pressure of the surrounding molecular cloud. If the jets are thermally confined, the thermal pressure internal to the jets is given by

$$P_j = n_j k T_j \approx n_c k T_c \, . \tag{16}$$

Balancing the thermal pressure of the jets with the magnetic pressure of the surrounding cloud gives

$$n_c k T_c = \frac{B^2}{8\pi} \, , \tag{17}$$

and hence a magnetic field strength of

$$B \approx 30 \left[\frac{n_c}{10^4 \text{ cm}^{-3}}\right]^{1/2} \left[\frac{T_c}{30 \text{ K}}\right]^{1/2} \mu\text{G} \, . \tag{18}$$

The jets can therefore be magnetically confined only if $B > 30$ $\mu$G. Considering that the mean field in the general interstellar medium is a few $\mu$G, and that the field strength should be significantly larger in the cores of molecular clouds (due to the freezing of the field lines during the collapse of molecular clouds to form cloud cores), the requirement of a few tens of $\mu$G is not unrealistic. A direct measurement of the strength and direction of the magnetic fields within the DR 21 cloud is therefore of fundamental importance to our understanding of the jet collimation mechanism in this particular outflow source.

In conclusion, it appears that the highly collimated $H_2$ jets associated with the DR 21 star-forming region probably result from the confinement of a high-velocity stellar wind by the thermal pressure of the ambient cloud medium. However, it is important to note that if $B > 30$ $\mu$G, the magnetic pressure will play a dominant role in confining the jets. Both the adiabatic and cooling jet models predict oscillations of the jet boundary which in turn may form oblique shocks internal to the jets. This may explain an origin for the periodic clumping of the $H_2$ emission that is clearly present in the western jet. Such oscillations may also produce the sudden shifts in the velocity of peak $H_2$ line emission along the western jet, as illustrated in Figure 4. Alternatively, sudden changes in both direction and velocity of the $H_2$ emission may result if the jet collides with numerous dense clumps in the surrounding ambient cloud medium. The origin of the bends and radial velocity shifts will be discussed in more detail in Papers III and IV.

## V. CONCLUSIONS

The DR 21 molecular cloud complex has been mapped, at reasonably high-spectral resolution, in the $v = 1$–$0$ $S(1)$ transition of molecular hydrogen. These observations reveal the existence of a highly collimated, bipolar flow consisting of two large and massive lobes of shocked, hypersonically expanding molecular gas. This is the largest and most luminous, in $H_2$ line emission, of all the molecular outflow sources known to date.

The DR 21 $H_2$ emission-line jets are dissimilar with regard to their kinematic structure: the east jet has relatively narrow lines ($<20$ km s$^{-1}$) while the west jet exhibits profiles with velocity widths that exceed 100 km s$^{-1}$. In the latter case, the highest velocity emission may arise from cloudlets of dense gas which move outward at almost the flow velocity, whereas the intense emission that characterizes the line-core probably originates from shocked ambient gas that is swept-up to form a dense, slow-moving shell bordering the expansion region. We believe that the supersonic gas that fills the jets and drives the observed shocks is composed primarily of a warm ($>100$ K), medium-density ($>100$ cm$^{-3}$), high-velocity ($>100$ km s$^{-1}$) atomic wind. If this is indeed the case, it is possible that the jets are confined by the thermal pressure of the surrounding ambient cloud medium. However, if the magnetic field strength is significantly greater than 30 $\mu$G, it is possible that the jets may be magnetic-pressure confined.

The detailed internal structure of the west jet, as delineated by the $H_2$ line emission, indicates the presence of a clumpy medium. In this medium, the brightest peaks of $H_2$ line emission are periodically spaced along the jet axis in a remarkably regular fashion. This periodic clumping is suggestive of laboratory measurements and theoretical models of pressure-confined, fluid-dynamical jets that are commonly employed to explain the observed morphology of extragalactic plasma jets.

The large-scale collimation mechanism operative in the DR 21 molecular cloud may therefore involve unstable pressure confinement after sudden ejection from a De Laval nozzle formed at the outer boundary of the dense cloud core. In such a model, the presence of substantial lateral motions within the jet excite a train of oblique shocks, the interaction of which results in the formation of a series of compression and rarefaction regions which are periodically spaced along the jet. The shock-excited $H_2$ emission-line clumps may then be associated with the compression regions, where the oblique shocks converge, and the gaps with the rarefaction regions, where the jet expands freely and cools rapidly. A detailed high-angular resolution study of the spatial distribution, shape and velocity of the shock-excited emission-line knots is necessary in order to test this hypothesis.

REFERENCES


Bally, J., and Lada, C. J. 1983, *Ap. J.*, **265**, 824.
Beckwith, S. 1980, in *IAU Symposium 96, Infrared Astronomy*, ed. C. G. Wynn-Williams and D. P. Cruikshank (Dordrecht: Reidel), p. 167.
Beckwith, S., Evans, N. J. II, Gatley, I., Gull, G., and Russell, R. W. 1983, *Ap. J.*, **264**, 152.
Blandford, R. D., and Konigl, A. 1979, *Ap. J.*, **232**, 34.
Blandford, R. D., and Rees, M. 1974, *M.N.R.A.S.*, **169**, 395.
Canto, J., and Rodriguez, L. F. 1980, *Ap. J.*, **239**, 982.
Canto, J., Tenorio-Tagle, G., and Rozyczka, M. 1988, *Astr. Ap.*, **192**, 287.
Dyson, J. E. 1984, *Ap. Space Sci.*, **106**, 181.
Geballe, T. R., and Garden, R. P. 1987, *Ap. J. (Letters)*, **317**, L107.
Garden, R. P., Geballe, T. R., Gatley, I., and Nadeau, D. 1986, *M.N.R.A.S.*, **220**, 203 (Paper I).
Garden, R. P., Russell, A. P., and Burton, M. G. 1990, *Ap. J.*, **354**, 232.
Hardee, P. E. 1982, *Ap. J.*, **257**, 509.
Harris, S. 1973, *M.N.R.A.S.*, **162**, 5p.
Hartmann, L., and Lazarus, F. 1941, *Phil. Mag.*, **31**, 35.
Harvey, P. M., Campbell, M. F., and Hoffmann, W. F. 1977, *Ap. J.*, **211**, 786.
Harvey, P. M., Joy, M., Lester, D. F., and Wilking, B. A. 1986, *Ap. J.*, **300**, 737.
Hough, J. H., Allen, D., Bailey, J., Burton, M. G., Garden, R. P., and Gatley, I. 1987, *M.N.R.A.S.*, **222**, 629.
Konigl, A. 1982, *Ap. J.*, **261**, 115.
Kwok, S., and Volk, K. 1985, *Ap. J.*, **299**, 191.
Lada, C. J. 1986, *Ann. Rev. Astr. Ap.*, **23**, 276.
Lane, A. P., and Bally, J. 1986, *Ap. J.*, **310**, 820.
Mundt, R., Brugel, E. W., and Buhrke, T. 1987, *Ap. J.*, **319**, 275.
Nadeau, D., and Geballe, T. R. 1990, in preparation.
Nadeau, D., Geballe, T. R., and Neugebauer, G. 1982, *Ap. J.*, **253**, 154.
Norman, C., and Silk, J. 1980, *Ap. J.*, **238**, 158.
Norman, M. L., Smarr, L., Wilson, J. R., and Smith, M. D. 1981, *Ap. J.*, **247**, 52.
Norman, M. L., Smarr, L., and Winkler, K. A. 1986, in *Numerical Astrophysics*, ed. J. M. Centrella, J. M. LeBlanc, and R. L. Bowers (Boston: Jones and Bartlett).
Prandtl, M. 1904, *Phys. Z.*, **5**, 599.
Roelfsema, P. R., Goss, W. M., and Geballe, T. R. 1989, *Astr. Ap.*, **222**, 247.
Rozyczka, M., and Tenorio-Tagle, G. 1985, *Astr. Ap.*, **147**, 209.
Russell, A. P. G. 1990, in *Submillimeter Astronomy*, ed. G. D. Watt and A. S. Webster (Dordrecht: Kluwer), p. 281.
Sanders, R. H. 1983, *Ap. J.*, **266**, 73.
Scoville, N. Z., Hall, D. N. B., Kleinmann, S. G., and Ridgway, S. T. 1982, *Ap. J.*, **253**, 136.
Skilling, J., and Bryan, P. K. 1984, *M.N.R.A.S.*, **211**, 111.
Tenorio-Tagle, G. 1979, *Astr. Ap.*, **71**, 59.
Willingdale, R. 1981, *M.N.R.A.S.*, **194**, 359.
Wilson, M. J., and Falle, A. E. G. 1985, *M.N.R.A.S.*, **216**, 971.



R. P. Garden: Department of Physics, University of California, Irvine, CA 92717

I. Gatley: National Optical Astronomy Observatories, P.O. Box 26732, Tucson, AZ 85726-6732

T. R. Geballe: Joint Astronomy Center, 665 Komohana Street, Hilo, HI 96720

D. Nadeau: University de Montreal, Department de Physique, CP 6128, Succ. A, Montreal, Canada PQ H3C 3J7